Scripta Materialia 241 (2024) 115889

Contents lists available at ScienceDirect

Scripta Materialia

journal homepage: www.journals.elsevier.com/scripta-materialia

Size-effects in tensile fracture of rejuvenated and annealed metallic glass

Akib Jabed, Golden Kumar *

Department of Mechanical Engineering, The University of Texas at Dallas, Richardson, TX 75080, USA

ARTICLE INFO

Keywords:
Metallic glass
Shear bands
Size-effects
Rejuvenation

ABSTRACT

Hundreds of Pt-based metallic glass samples with diameters ranging from sub-100 nm to 100 μm are subjected to cryogenic rejuvenation and annealing above glass transition temperature before tensile loading at room temperature. Shear-localized failure with no ductility is observed in large samples whereas the smaller diameter specimens show ductile necking irrespective of the structural state of metallic glass. With decreasing sample diameter, the fracture surface changes from vein pattern to featureless in the shear-localized samples and the ductility increases in the necked samples. Despite similar size-dependent trends, the changes in deformation mode and fracture morphology occur at different diameters in as-cast, rejuvenated, and annealed samples. The critical diameters for transitions from shear localization to necking and from vein pattern to smooth fracture surface shift to larger values in cryogenically rejuvenated samples whereas annealing has the opposite effect. Rejuvenation promotes homogeneous-like flow and suppresses catastrophic tensile failure in nanoscale metallic glasses.

Plastic deformation in metallic glasses (MGs) at room temperature is localized in 10–20 nm thick shear bands due to strain softening [1–8]. While multiple shear bands can form and accommodate plastic strain during the compression and bending of MGs, a single shear band results in catastrophic failure in uniaxial tension [9–13]. Lack of ductility is the major concern for applications that could benefit from the unique properties and processing capabilities of MGs. Various approaches such as ductile reinforcement [14–16], cold rolling [17], and structural modification [18] have been studied to enhance the plasticity of MGs. These strategies are effective in increasing the shear band mediated plasticity under constrained loading conditions whereas the tensile ductility remains negligible except in MG composites. Incorporating ductile crystalline phase can mitigate the brittleness of MGs but it also diminishes the attractive properties of monolithic MGs.

Numerous studies have shown that extreme shear localization can be averted in nanoscale MGs [19–23]. Departure from shear banding results in necking and substantial ductility in tensile deformation of nanoscale MGs [24,25]. Homogeneous-like plastic deformation in MGs has generated significant interest due to potential applications and advancement in understanding the plastic flow in amorphous solids [19,21,22,26–33]. However, the existence and mechanism of size-dependent plasticity in MGs have remained contentious because of focused-ion-beam (FIB) sample preparation artifacts and limited experimental data [25,27,29,32,33]. The sensitivity of glassy structure to cooling rate and irradiation further complicates the interpretation of size-effects in MGs.

Recent studies have focused on the structural rejuvenation of MGs by thermal cycling between the cryogenic and room temperatures to increase plasticity [34–37]. It has been shown that with an optimal number of cryogenic cycles, a significant enhancement in the plasticity of some MGs can be achieved through the proliferation of shear bands [34]. The structural rejuvenation is not monotonic, and excessive cryogenic thermal cycling can result in embrittlement of certain MGs [38]. The effect of rejuvenation has been mostly investigated on the compressive plasticity and fracture toughness of MGs but results also suggest potential benefits in tensile deformation [39]. Rejuvenation can counter extensive strain localization by promoting multiple shear bands in MG subjected to tension [39,40]. However, the effect of structural rejuvenation on the tensile ductility of bulk samples is limited [39]. Therefore, it is intriguing to study if structural rejuvenation can be combined with size-effects to improve the tensile ductility of nanoscale MGs. Due to experimental challenges, structural rejuvenation has not been applied to nanoscale MG samples. The present work investigates the effect of structural rejuvenation on tensile fracture of small-scale MG specimens. Annealing above the glass transition temperature (T_g) is also studied to understand the overall role of the structural state in size-effects in MGs.

Pt-based alloy $Pt_{57.5}Cu_{14.7}Ni_{5.3}P_{22.5}$ (at.%) was prepared by melting

* Corresponding author.
E-mail address: golden.kumar@utdallas.edu (G. Kumar).

https://doi.org/10.1016/j.scriptamat.2023.115889
Received 31 August 2023; Received in revised form 14 November 2023; Accepted 15 November 2023

of high purity elements in a vacuum-sealed quartz tube. The crystalline ingot was fluxed with B_2O_3 at 1000 °C followed by water quenching to obtain a cylindrical MG sample with a 2 mm diameter. The glassy state of the as-cast sample was verified by comparing the differential scanning calorimetry results with literature values. Damage-free tensile specimens from Pt-based metallic glass (Pt-MG) were prepared by thermoplastic drawing as schematically illustrated in Fig. 1. More details of thermoplastic drawing setup and experimental conditions can be found elsewhere [41]. In brief, the Pt-MG was pressed and pulled against mold cavities at 265 °C (T_g = 230 °C). Silicon and aluminum molds with cavity diameters ranging from 10 to 500 μm were used to draw MG wires with controllable diameters from sub-100 nm to 100 μm. The drawn samples were cooled to room temperature which will be hereafter referred to as "as-cast". One set of the as-cast samples was subjected to 15 cryogenic cycles between liquid nitrogen and room temperature to induce structural rejuvenation. Each cryogenic cycle consisted of submerging in liquid nitrogen for 1 min followed by holding for 1 min at room temperature. The bulk samples of Pt-MG exhibit maximum rejuvenation at about 25 cryogenic cycles [42]. To avoid potential embrittlement due to excessive thermal cycling, only 15 cryogenic cycles were selected for nanoscale Pt-MG samples. Another set of as-cast samples was annealed at 270 °C for 12 min which is shorter than the crystallization onset time of 20 min reported in the bulk samples [43]. The transmission electron microscopy (TEM) studies on samples of 120 nm and 20 μm diameters showed no detectable crystals after annealing (Fig. S1). The as-cast, cryogenically rejuvenated, and above-T_g annealed MG samples of varying diameters were fractured in tension at room temperature (Fig. 1). Hundreds of fractured samples with three different structural states were analyzed using SEM images to understand the effects of structural state and sample size on tensile deformation. The fractured specimens showed two distinct deformation modes: shear localization and necking. The shear-localized mode is characterized by catastrophic failure at an angle of about 50–55° with no ductility. The necked samples displayed a significant reduction in sample diameter accompanied by large plastic strain. The size-dependent transition from shear localization to necking is affected by the structural state of MG.

Fig. 2 compares the size-dependent fracture morphology of representative Pt-MG samples with different structural states. The samples with large diameters fracture along a single shear band and the fracture surface consists of a featureless area and vein-pattern. The veins diminish with decreasing sample diameter while the plastic deformation remains localized in a single shear band with no global tensile ductility. The fracture morphology changes from planar to rugged and subsequently to necking with decreasing sample diameter. Here, "planar" morphology refers to catastrophic failure along a single shear band at an angle of about 50–55° whereas "rugged" morphology characterizes the zig-zag fracture surface due to failure along multiple planes at different angles. The overall size-dependent changes in tensile deformation of Pt-MG are similar for three structural states but the transitions occur at different diameters. The fracture surface of the annealed sample with a diameter of 10 μm is largely covered with veins whereas the as-cast and the rejuvenated samples show significant fractions of smooth areas on their fracture surfaces. The rejuvenated sample of diameter 5 μm displays a featureless fracture surface, but veins are clearly visible in the as-cast and the annealed samples. A completely smooth fracture surface is only observed at diameters below 2 μm and 800 nm for the as-cast and the annealed states, respectively. Furthermore, the vein morphology in annealed samples is different from the as-cast and the rejuvenated specimens. The veins have no preferential orientation in the case of annealed samples whereas the as-cast and the rejuvenated samples show one central vein with nearly parallel branches. The formation of veins and smooth shear-offset is the combined effect of normal and shear stresses in the fracture of MGs. The fractographic features suggest that the contribution of normal stress is higher in annealed samples with large diameters compared to the as-cast and rejuvenated samples.

The tensile fracture morphology changes from planar to rugged with decreasing sample diameter. The plastic deformation in MGs becomes increasingly delocalized at smaller sample diameters as indicated by the necking and permanent elongation. The size-dependent transition from localized shear banding to homogenous-like deformation has been the subject of size-effect studies in MGs [19,21,24–31]. The existence of homogeneous flow in MGs at room temperature has been disputed due to potential sample preparation artifacts such as FIB damage [25,32,33,44,45]. The dimensional constraint perpendicular to the loading direction in nanoscale samples can result in multiaxial stress state as demonstrated by the previous studies on notched specimens [31,46].

The current results from hundreds of FIB-free tensile samples confirm that the necking in nanoscale MGs exists and the onset of necking transition is affected by the structural state of MG (Fig. 2). The as-cast sample of 400 nm diameter displays rugged fracture morphology without noticeable plasticity whereas the rejuvenated specimen necks down with significant plastic deformation. In contrast, the annealed sample of the same diameter fractures along a dominant shear band. The 100 nm diameter samples in all three structural states show necking and

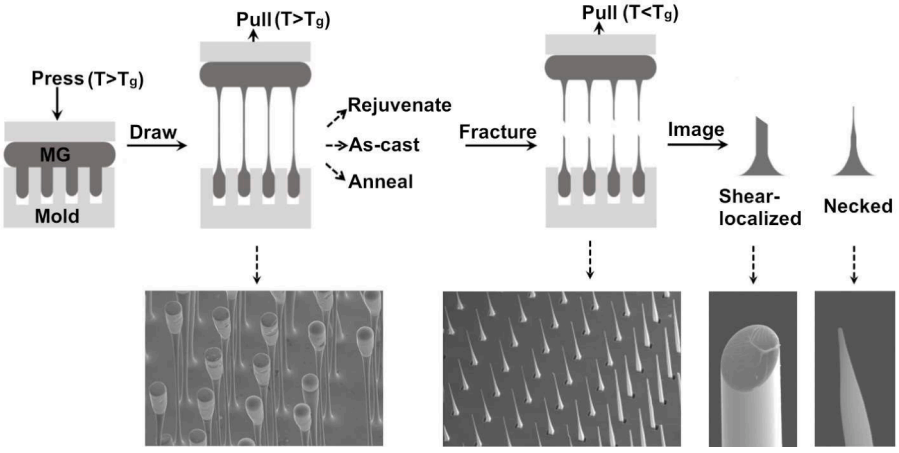

Fig. 1. Schematic illustration of FIB-free fabrication and testing of MG tensile specimens with different structural states. The MG was pressed and pulled against a mold heated above T_g resulting in a thermoplastic drawing of multiple dog-bone-shaped samples with controllable diameters ranging from sub-100 nm to 100 μm. The drawn samples were subjected to cryogenic cycling and above-T_g isothermal treatments to generate rejuvenated and annealed structural states, respectively. The untreated samples referred to as "as-cast" were also studied for comparison. The samples with different structural states were fractured in tension at room temperature. Multiple fractured samples were imaged in SEM to characterize the size-dependent deformation mode (shear-localized or necking) in three structural states of MG. Representative SEM images of Pt-MG samples in as prepared state and after fracture are shown.

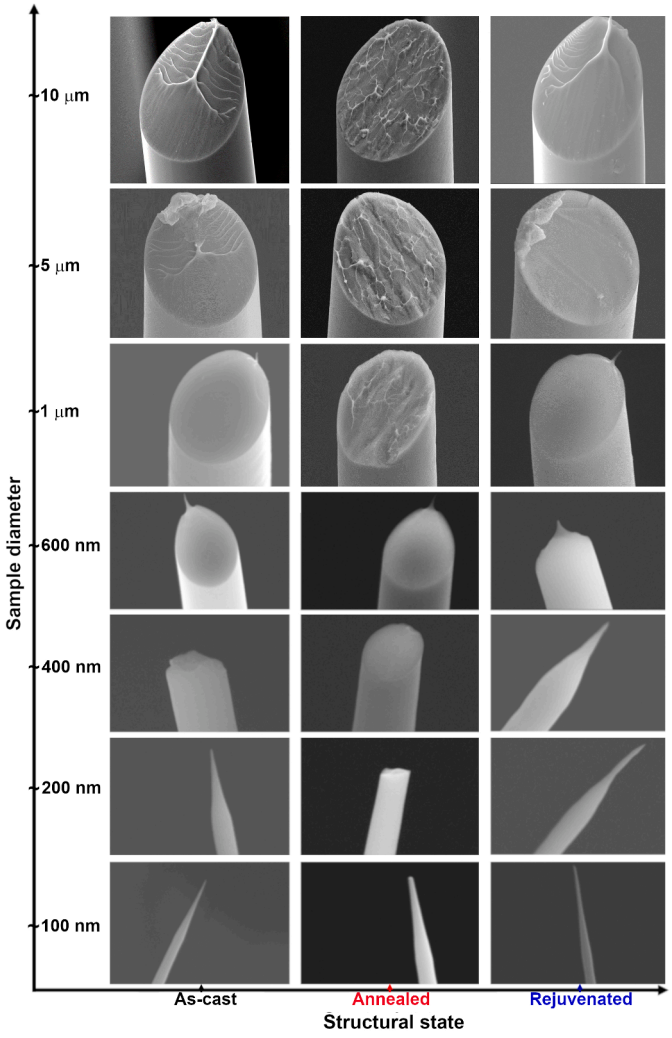

Fig. 2. SEM micrographs of tensile fracture surfaces of as-cast, rejuvenated, and annealed Pt-MG samples with varying diameters. Two types of fracture morphologies are observed as a function of sample diameter: shear-localized (planar) and necking. In shear-localized samples, the fracture surface changes from vein-pattern to completely smooth with decreasing diameter but the transition is affected by the structural state. The transition from planar fracture to necking is also sensitive to the structural state of MG.

ductile failure but the rejuvenated sample displays a higher propensity for necking with a longer neck length.

Multiple Pt-MG samples in different structural states were tested and the tensile fractographic features were measured to quantify the size-effects. The observed size-effects are divided into two categories: the changes in fractographic features of shear-localized samples and the change in the fracture mode from planar to necking. The fracture surfaces of shear-localized samples were analyzed by measuring the fractions of smooth and vein pattern areas. The smooth part of the fracture surface was estimated by shear-offset (δ) projected on a plane perpendicular to the loading direction as illustrated in Fig. 3a. The appearance of rugged fracture morphology was marked as the transition from shear localization. Fig. 3a shows the variation in normalized shear-offset (δ/d) as a function of sample diameter (d). The δ/d increases with decreasing sample diameter for all three structural states. However, the δ/d values are consistently higher for the rejuvenated samples and lowest for the annealed samples for each diameter. The transition from veins to a completely smooth fracture surface ($\delta/d = 1$) is also affected by the structural state of MG. Rejuvenation shifts the transition to a larger diameter whereas annealing has the opposite effect (arrows in Fig. 3a).

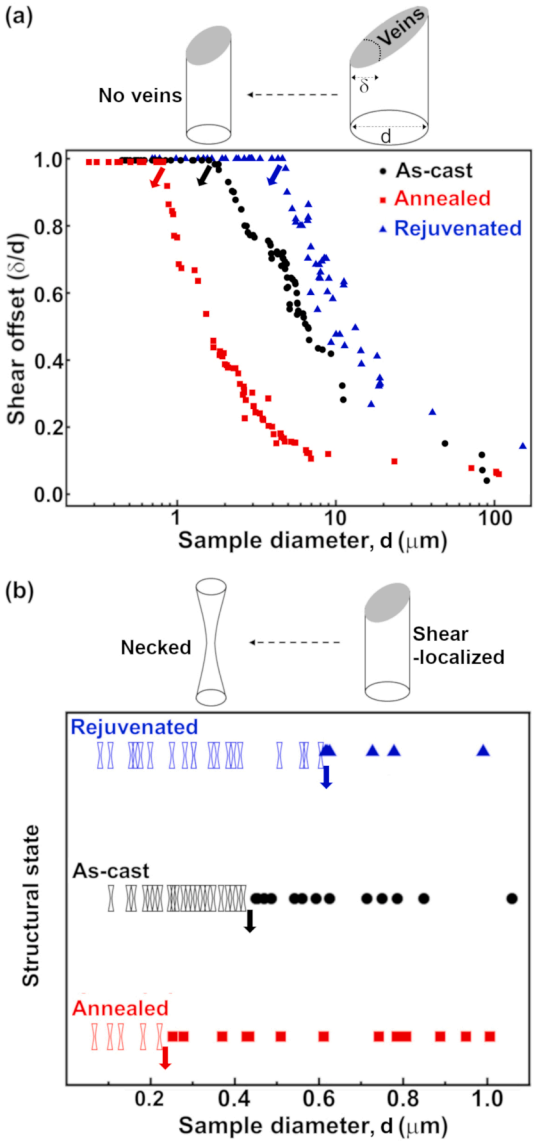

Fig. 3. Quantification of size-dependent changes in tensile fracture of Pt-MG samples in different structural states. (a) The normalized shear-offset δ represents the fraction of smooth area in the tensile fracture surface of shear-localized samples. The appearance of a completely smooth fracture surface is marked with arrows. (b) The transition from shear-localized planar fracture to homogeneous necking. Rejuvenation shifts both transitions (veins to smooth fracture and shear-localized to necking) to larger diameters while annealing has the opposite effect.

The smooth region in the tensile fracture surface of MGs is attributed to the cooperative sliding of two parts across a major shear band before the final fracture occurs due to formation of liquid-like layer. The vein pattern stems from the Saffman-Taylor instability of the liquid layer formed due to heating [9]. Therefore, an increase in δ/d indicates suppression of heating and liquid layer formation with decreasing sample diameter and structural rejuvenation.

The transition from shear-localized fracture to necking in Pt-MG samples is plotted in Fig. 3b. The samples with a localized planar fracture surface show no signs of macroscopic plastic deformation whereas the necked specimens display a significant reduction in sample diameter before fracture. The departure from single shear band mediated fracture is observed below a critical sample diameter of about 430 nm in the as-cast state. This critical diameter increases to 610 nm upon structural rejuvenation and decreases to 220 nm after annealing. The extent of

necking below critical diameter also varied with the structural state of MG. To quantify the necking, true strain ($\varepsilon_T = \ln(d^2/d_n^2)$) values were calculated as a function of distance (L/d) following the approach used by Yi et al. [25]. Here d_n is the neck diameter at a distance L from the point of fracture (Fig. 4a). The ε_T values for samples of 300 nm and 150 nm diameters with different structural states are plotted in Fig. 4a and Fig. 4b, respectively. The SEM images of fractured specimens used for the calculation of ε_T are also shown in Fig. 4. The ε_T remains zero for the annealed sample of 300 nm diameter which failed along a dominant shear band without necking (Fig. 4a). In contrast, the as-cast and the rejuvenated samples exhibit clear necking with ε_T gradually decreasing to zero with increasing distance from the fracture point. The neck half-length can be calculated from the L/d value at which ε_T becomes zero. The rejuvenated sample forms a longer and thinner neck indicating higher tensile ductility compared to the as-cast sample. The same trend continues for 150 nm diameter samples in which necking is observed for all three structural states (Fig. 4b). The annealed specimen fractures with a short neck (half-length ~ 375 nm) whereas the rejuvenated sample forms a long neck (half-length ~ 900 nm). These results show that structural rejuvenation by thermal cycling enhances the tensile ductility in MGs.

The ability to suppress catastrophic tensile failure in large samples by post-processing is desirable for MGs. Annealing typically results in embrittlement due to structural relaxation or crystallization whereas rejuvenation enhances plasticity in MGs [47]. Rejuvenated MGs show a higher number of smaller shear bands resulting in improved compressive or bending plasticity, but tensile ductility remains negligible due to single shear band dominated failure [34]. In a recent study, Zhou et al. showed that extreme structural rejuvenation achieved under triaxial stress can avert catastrophic tensile failure along a single major shear band [39,40]. A rugged tensile fracture surface was observed indicating the activation of multiple shear bands in the rejuvenated samples [39]. The departure from the single shear band was attributed to structural relaxation induced strain-hardening under tension. Strain-hardening and rugged tensile fracture were also previously reported by Joo et al. in Zr-based MG subjected to high-pressure torsion [48]. Despite the suppression of runaway shear band, the full potential of structural rejuvenation has not been realized in bulk samples of MGs, which fail below 1 % plastic strain by shear banding. In contrast, the present work shows that structural rejuvenation in nanoscale MGs can completely suppress the major shear bands resulting in large plastic strain and necking.

The results also indicate a clear synergy between the sample size and the structural state in governing the tensile fracture of MG. Structural rejuvenation and smaller sample size promote shear delocalization but annealing and increasing sample size cause catastrophic failure along a dominant shear band. These observations suggest a similarity between the underlying mechanisms for the suppression of catastrophic tensile failure by structural rejuvenation and reduction in sample size. While the effect of rejuvenation has been explained by strain-hardening, the origin of size-dependent change in deformation mode has remained elusive. The shear band formation and propagation in MGs has been associated with strain-softening [1,2,5]. The strain-softening is countered by structural relaxation in rejuvenated MGs but the mitigation of strain-softening in as-cast nanoscale MGs is not understood. We hypothesize that the shear localization in nanoscale MGs is prevented by the lack of heating and enhanced atomic mobility. The results indicate that the heat generated during plastic deformation of MGs is lower in smaller samples as manifested by the shrinking vein pattern area on the fracture surface. Below a critical sample size, the heat is not sufficient to form a major shear band across the MG sample. Shimizu et al. proposed that a critical length of the embryonic shear band and a rise in temperature are required to nucleate a major shear band [49]. The amount of heat generated during plastic deformation is expected to decrease with structural rejuvenation because of a decrease in yield strength. Therefore, both structural rejuvenation and reduction in sample size can

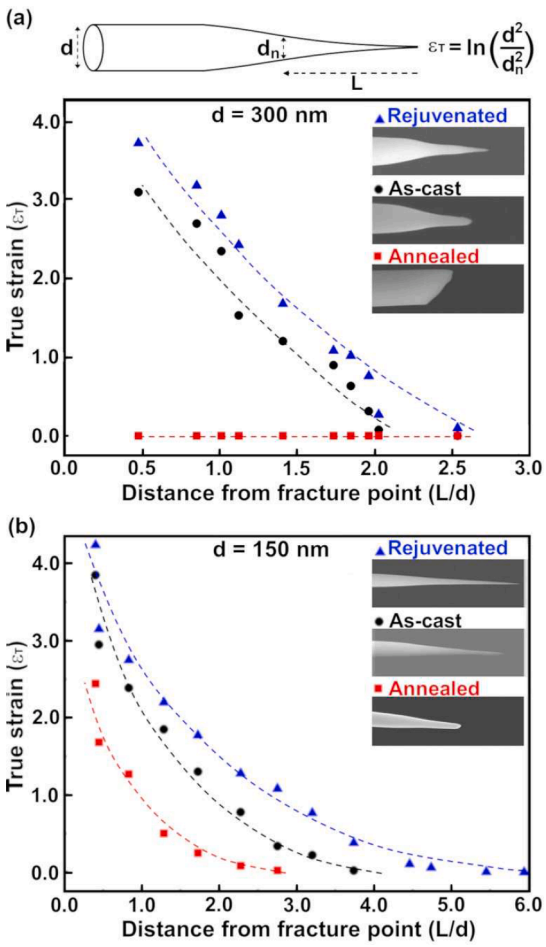

Fig. 4. True strain ε_T values calculated (as depicted above) as a function of normalized distance L from the point of fracture in necked Pt-MG samples in different structural states for two diameters: (a) 300 nm and (b) 150 nm. The SEM images of the fractured specimens with different structural states are shown in the inset. The rejuvenated specimens form longer and thinner necks for both diameters.

prevent major shear banding in MGs as observed in the current study. It is worth noting that strain-hardening has been reported by Jang et al. [24] and Tian et al. [50] in tensile testing nanoscale MGs however it was not correlated to the suppression of shear localization. While strain-hardening was not measured in the current study, further work is needed to investigate the role of strain-hardening in the size-dependent changes observed in the deformation mode of MGs.

In addition, the structural disorder generated by plastic deformation is effectively annihilated in nanoscale MGs by higher atomic mobility thus preventing the shear localization. Recent study showed that higher atomic mobility in small-scale MGs can result in lower fictive temperature [51]. It is important to note that structural rejuvenation alone is not sufficient to induce tensile necking in bulk MGs where the final fracture sill occurs through major shear bands [39]. In contrast, structural rejuvenation in combination with reduced sample size can suppress the localization in major shear bands resulting in necking. Therefore, a combination of sample size and structural state can be utilized to prevent catastrophic tensile failure in MGs.

Declaration of Competing Interest

The authors declare that they have no known competing financial interests or personal relationships that could have appeared to influence the work reported in this paper.

Acknowledgment

The work was supported by the National Science Foundation (NSF) through CMMI NSF-CAREER Award#1921435.

Supplementary materials

Supplementary material associated with this article can be found, in the online version, at doi:10.1016/j.scriptamat.2023.115889.

References

[1] C.A. Schuh, T.C. Hufnagel, U. Ramamurty, Overview No.144 - mechanical behavior of amorphous alloys, Acta Mater. 55 (2007) 4067–4109.
[2] A.L. Greer, Y.Q. Cheng, E. Ma, Shear bands in metallic glasses, Mater. Sci. Eng. Rep. 74 (2013) 71–132.
[3] B.A. Sun, W.H. Wang, The fracture of bulk metallic glasses, Prog. Mater. Sci. 74 (2015) 211–307.
[4] J.J. Lewandowski, W.H. Wang, A.L. Greer, Intrinsic plasticity or brittleness of metallic glasses, Philos. Mag. Lett. 85 (2005) 77–87.
[5] R. Maass, F. Loffler, Shear-band dynamics in metallic glasses, Adv. Funct. Mater. 25 (2015) 2353–2368.
[6] X. Xie, Y.C. Lo, Y. Tong, J. Qiao, G. Wang, S. Ogata, H. Qi, K.A. Dahmen, Y. Gao, P. K. Liaw, Origin of serrated flow in bulk metallic glasses, J. Mech. Phys. Solids 124 (2019) 634–642.
[7] S.X. Song, T.G. Nieh, Direct measurements of shear band propagation in metallic glasses - an overview, Intermetallics 19 (2011) 1968–1977.
[8] R. Maass, D. Klaumunzer, J.F. Loffler, Propagation dynamics of individual shear bands during inhomogeneous flow in a Zr-based bulk metallic glass, Acta Mater. 59 (2011) 3205–3213.
[9] Z.F. Zhang, J. Eckert, L. Schultz, Difference in compressive and tensile fracture mechanisms of Zr59Cu20Al10Ni8Ti3 bulk metallic glass, Acta Mater. 51 (2003) 1167–1179.
[10] R.D. Conner, Y. Li, W.D. Nix, W.L. Johnson, Shear band spacing under bending of Zr-based metallic glass plates, Acta Mater. 52 (2004) 2429–2434.
[11] J. Das, M.B. Tang, K.B. Kim, R. Theissmann, F. Baier, W.H. Wang, J. Eckert, Work-hardenable" ductile bulk metallic glass, Phys. Rev. Lett. 94 (2005), 205501.
[12] G. Kumar, T. Ohkubo, T. Mukai, K. Hono, Plasticity and microstructure of Zr-Cu-Al bulk metallic glasses, Scr. Mater. 57 (2007) 173–176.
[13] R.T. Qu, M. Stoica, J. Eckert, Z.F. Zhang, Tensile fracture morphologies of bulk metallic glass, J. Appl. Phys. 108 (2010).
[14] D.C. Hofmann, J.Y. Suh, A. Wiest, G. Duan, M.L. Lind, M.D. Demetriou, W. L. Johnson, Designing metallic glass matrix composites with high toughness and tensile ductility, Nature 451 (2008) 1085–1089.
[15] M.L. Lee, Y. Li, C.A. Schuh, Effect of a controlled volume fraction of dendritic phases on tensile and compressive ductility in La-based metallic glass, Acta Mater. 52 (2004) 4121–4131.
[16] Z. Zhu, H. Zhang, Z. Hu, W. Zhang, A. Inoue, Ta-particulate reinforced Zr-based bulk metallic glass matrix composite with tensile plasticity, Scr. Mater. 62 (2010) 278–281.
[17] Y. Yokoyama, K. Inoue, K. Fukaura, Cold-rolled Zr50Cu30Ni10Al10 bulk amorphous alloys with tensile plastic elongation at room temperature, Mater. Trans. 43 (2002) 3199–3205.
[18] E. Ma, J. Ding, Tailoring structural inhomogeneities in metallic glasses to enable tensile ductility at room temperature, Mater. Today 19 (2016) 568–579.
[19] H. Guo, P.F. Yan, Y.B. Wang, J. Tan, Z.F. Zhang, M.L. Sui, E. Ma, Tensile ductility and necking of metallic glass, Nat. Mater. 6 (2007) 735–739.
[20] D. Tonnies, R. Maass, C.A. Volkert, Room temperature homogeneous ductility of micrometer-sized metallic glass, Adv. Mater. 26 (2014) 5715–5721.
[21] C.A. Volkert, A. Donohue, F. Spaepen, Effect of sample size on deformation in amorphous metals, J. Appl. Phys. 103 (2008), 083539.
[22] A. Bharathula, S.W. Lee, W.J. Wright, K.M. Flores, Compression testing of metallic glass at small length scales: effects on deformation mode and stability, Acta Mater. 58 (2010) 5789–5796.
[23] C. Zhong, H. Zhang, Q.P. Cao, X.D. Wang, D.X. Zhang, J.W. Hu, P.K. Liaw, J. Z. Jiang, Non-localized deformation in Cu-Zr multi-layer amorphous films under tension, J. Alloy. Compd. 678 (2016) 410–420.
[24] D.C. Jang, J.R. Greer, Transition from a strong-yet-brittle to a stronger-and-ductile state by size reduction of metallic glasses, Nat. Mater. 9 (2010) 215–219.
[25] J. Yi, W.H. Wang, J.J. Lewandowski, Sample size and preparation effects on the tensile ductility of Pd-based metallic glass nanowires, Acta Mater. 87 (2015) 1–7.
[26] C.S. Meduri, J. Blawzdziewicz, G. Kumar, Size-temperature equivalence in tensile deformation of metallic glass, Mater. Sci. Eng. A Struct. 805 (2021), 140595.
[27] A. Dubach, R. Raghavan, J.F. Loffler, J. Michler, U. Ramamurty, Micropillar compression studies on a bulk metallic glass in different structural states, Scr. Mater. 60 (2009) 567–570.
[28] F.F. Wu, Z.F. Zhang, S.X. Mao, Size-dependent shear fracture and global tensile plasticity of metallic glasses, Acta Mater. 57 (2009) 257–266.
[29] B.E. Schuster, Q. Wei, T.C. Hufnagel, K.T. Ramesh, Size-independent strength and deformation mode in compression of a Pd-based metallic glass, Acta Mater. 56 (2008) 5091–5100.
[30] Z.W. Shan, J. Li, Y.Q. Cheng, A.M. Minor, S.A. Syed Asif, O.L. Warren, E. Ma, Plastic flow and failure resistance of metallic glass: insight from *in situ* compression of nanopillars, Phys. Rev. B 77 (2008), 155419.
[31] R.L. Narayan, L. Tian, D. Zhang, M. Dao, Z.W. Shan, K.J. Hsia, Effects of notches on the deformation behavior of submicron sized metallic glasses: insights from *in situ* experiments, Acta Mater. 154 (2018) 172–181.
[32] R. Raghavan, K. Boopathy, R. Ghisleni, M.A. Pouchon, U. Ramamurty, J. Michler, Ion irradiation enhances the mechanical performance of metallic glasses, Scr. Mater. 62 (2010) 462–465.
[33] D.J. Magagnosc, G. Kumar, J. Schroers, P. Felfer, J.M. Cairney, D.S. Gianola, Effect of ion irradiation on tensile ductility, strength and fictive temperature in metallic glass nanowires, Acta Mater. 74 (2014) 165–182.
[34] S.V. Ketov, Y.H. Sun, S. Nachum, Z. Lu, A. Checchi, A.R. Beraldin, H.Y. Bai, W. H. Wang, D.V. Louzguine-Luzgin, M.A. Carpenter, A.L. Greer, Rejuvenation of metallic glasses by non-affine thermal strain, Nature 524 (2015) 200–203.
[35] J. Pan, Y.X. Wang, Q. Guo, D. Zhang, A.L. Greer, Y. Li, Extreme rejuvenation and softening in a bulk metallic glass, Nat. Commun. 9 (2018) 9.
[36] M.B. Costa, J.J. London, A. Blatter, A. Hariharan, A. Gebert, M.A. Carpenter, A. L. Greer, Anelastic-like nature of the rejuvenation of metallic glasses by cryogenic thermal cycling, Acta Mater. 244 (2023), 118551.
[37] X. Li, J.G. Wang, H.B. Ke, C. Yang, W.H. Wang, Extreme rejuvenation and superior stability in a metallic glass, Mater. Today Phys. 27 (2022), 100782.
[38] J. Ketkaew, R. Yamada, H. Wang, D. Kuldinow, B.S. Schroers, W. Dmowski, T. Egami, J. Schroers, The effect of thermal cycling on the fracture toughness of metallic glasses, Acta Mater. 184 (2020) 100–108.
[39] W.H. Zhou, N.T. Panagiotopoulos, A.L. Greer, Y. Li, Strain-hardening under uniaxial tension in a rejuvenated bulk metallic glass, Scr. Mater. 212 (2022), 114572.
[40] J. Pan, Y.P. Ivanov, W.H. Zhou, Y. Li, A.L. Greer, Strain-hardening and suppression of shear-banding in rejuvenated bulk metallic glass, Nature 578 (2020) 559–562.
[41] S. Jagdale, A. Jabed, S. Theeda, C.S. Meduri, Z.L. Hu, M. Hasan, G. Kumar, Review of thermoplastic drawing with bulk metallic glasses, Metals 12 (2022) 518 (Basel).
[42] M.B. Costa, J.J. Londono, A. Blatter, A. Hariharan, A. Gebert, M.A. Carpenter, A. L. Greer, Anelastic-like nature of the rejuvenation of metallic glasses by cryogenic thermal cycling, Acta Mater. 244 (2023), 118551.
[43] A. Jabed, C.S. Meduri, G. Kumar, Effect of time on the isothermal viscosity of metallic glass supercooled liquids, J. Alloy Compd. 863 (2021), 158067.
[44] D. Sopu, A. Foroughi, M. Stoica, J. Eckert, Brittle-to-ductile transition in metallic glass nanowires, Nano Lett. 16 (2016) 4467–4471.
[45] Y.F. Shi, Size-independent shear band formation in amorphous nanowires made from simulated casting, Appl. Phys. Lett. 96 (2010), 121909.
[46] X.W. Gu, M.J. Zadeh, D.G. Chen, Z. Wu, Y.W. Zhang, D.J. Srolovitz, J.R. Greer, Mechanisms of failure in nanoscale metallic glass, Nano Lett. 14 (2014) 5858–5864.
[47] G. Kumar, D. Rector, R.D. Conner, J. Schroers, Embrittlement of Zr-based bulk metallic glasses, Acta Mater. 57 (2009) 3572–3583.
[48] S.H. Joo, D.H. Pi, A.D.H. Setyawan, H. Kato, M. Janecek, Y.C. Kim, S. Lee, H. S. Kim, Work-hardening induced tensile ductility of bulk metallic glasses via high-pressure torsion, Sci. Rep. 5 (2015) 9.
[49] F. Shimizu, S. Otega, J. Li, Theory of shear banding in metallic glasses and molecular dynamics calculations, Mater. Trans. 48 (2007) 2923.
[50] L. Tian, Y.Q. Cheng, Z.W. Shan, C.C. Wang, X.D. Han, J. Sun, E. Ma, Approaching the ideal elastic limit of metallic glasses, Nat. Commun. 3 (2012) 609.
[51] V. Di Lisio, I. Gallino, S.S. Riegler, M. Frey, N. Neuber, G. Kumar, J. Schroers, R. Busch, D. Cangialosi, Size-dependent vitrification in metallic glasses, Nat. Commun. 14 (2023) 4698.